JOURNAL OF MATERIALS SCIENCE 33 (1998) 2095–2101

Pressure infiltration of sol/gel processed short fibre ceramic matrix composites

HSIEN-KUANG LIU, WEN-SHYONG KUO*, BOR-HORNG LIN
*Departments of Mechanical Engineering and *Textile Engineering, Feng-Chia University Taichung, Taiwan*

Using pressure infiltration short fibre-reinforced ceramic matrix composites with uniform and dense microstructure can be made. Based upon this processing technique, composites composed of silica sol, alumina particles, and alumina short fibres were fabricated. The related processing parameters studied in this work include infiltration rate, fibre volume fraction V_f, particle size, and infiltrate viscosity. An optimal infiltration rate was 4 mm min^{-1}, at which rate the composite with V_f of 8.1% and particle size of 3 μm has the highest green density. An equilibrium between particle packing strength and applied load must be obtained during the infiltration to obtain high green density and composite strength. The influence of fibre volume fraction and particle size on composite green density is in a synergistic manner because it involves particle–fibre interactions, fibre–fibre interactions, and sedimentation. Furthermore, the increase of sol viscosity results in more sedimentation in the infiltrate and lower composite green density. The fracture toughness of composites is 38% higher than that of monolithic alumina. © *1998 Chapman & Hall*

1. Introduction

Ceramic materials have several advantages for engineering applications, such as high strength and hardness, excellent performance under elevated temperature and corrosive environment. Nevertheless, the inherent brittleness of ceramic materials has greatly restricted their performance. Therefore, the development of fibre-reinforced ceramic matrix composites has attracted considerable attention to maximize the composite fracture toughness.

Using the sol–gel method to manufacture ceramic matrix composites has several advantages, such as good mobility during processing, uniform microstructure, low sintering temperature, near-net-shape fabrication, and versatile in producing a variety of matrix materials [1–3]. However, a major concern of this processing approach is excessive shrinkage of matrix during drying which can lead to extensive matrix cracking. Using pressure infiltration, Liu and Parvizi-Majidi [4] have fabricated three-dimensional ceramic matrix composites with satisfactory density and uniformity. In their work, the addition of solid particles to the sol during sol–gel processing of ceramic matrix composites can increase composite green density and reduce cracking caused by drying stresses. Velamakanni and Lange [5] have shown that three conditions are required to achieve high packing density during pressure filtration of colloidal powders: (1) strong repulsive interparticle potentials; (2) a bimodal particle size distribution containing the optimum composition of coarse and fine particles; and (3) a slurry with high enough viscosity to prevent possible particles segregation due to sedimentation. Lange *et al.* [6] also found that green density of the composite decreases as the diameter ratio of particles to fibres increases, which inferred that particles have to be small to allow satisfactory fibre packing. Lange and coworkers [7] demonstrated that dry powders behave more like flocced slurry, i.e. the packing density is very sensitive to the applied pressure and is lower compared to dispersed slurries. Thus, pressure filtration is required to achieve high packing densities.

In this paper, a short fibre ceramic matrix composite was fabricated in which short fibres, as reinforcing elements, could provide an improved through-the-thickness stiffness/strength and a better ability to formulate complex shapes. The infiltrate is obtained by mixing silica sol, alumina powders, and alumina short fibres. A pressure infiltration apparatus incorporated with a MTS testing machine were used. The MTS testing machine provides the necessary pressure for infiltration and a controllable crosshead speed (infiltration rate). The processing parameters include infiltration rate, fibre volume fraction, viscosity of sol, and particle size of solid additions. Their effects on green density, infiltration pressure, drying behaviour, and mechanical properties are investigated.

2. Material processing and characterization

2.1. Sol and infiltrate preparation

The silica sol was prepared using a modified recipe of Klein's work [8]. In this recipe, tetraethyl-orthosilicate (TEOS), ethanol, deionized water and 7 wt % of HNO_3 were mixed at a volume ratio of 1:1:1.6:0.06. The amount of sol for one infiltration is 175 ml. All the

reaction of the mixture was at room temperature. The viscosity of sol was varied in order to study its effect on particle packing in green composites. All measurements of low-viscosity sols were performed in a cup and bob geometry (Model DV-II viscometer, Brookfield, Stoughtan, MA). The sol with viscosity 0.04 Pa s was obtained according to the procedure above, while sols with viscosities 0.051 Pa s and 0.086 Pa s are prepared by evaporating 250 ml and 350 ml sols, respectively, to 175 ml. However, the sol with viscosity higher than 0.086 Pa s can not be obtained because of gelation. The alumina powders (α-Al_2O_3, Bayer process, average particle diameters of 0.45, 1 and 3 μm, purity of particle of 99.9%, and a density of 2.7 g cm^{-3}) and alumina short fibres (Zircar ALBF-1, USA, average length of 3.2 mm, average diameter of 3 μm, and a density of 3.4 g cm^{-3}) were added to the sol to prepare the infiltrate. The infiltrate is further mixed both in ultrasonic bath and electromagnetic blender in turns until the fibres and powders in the infiltrate were dispersed uniformly and well wetted. The infiltrate suspension was controlled to maintain a solid content of 22.9 wt %. The fibre volume fraction V_f in infiltrate was predetermined as 8.1, 16.6 and 25.4%.

2.2. Pressure infiltration and consolidation

As shown in Fig. 1, the apparatus for pressure infiltration consists of a plunger, a cylinder with an inner diameter of 50 mm, a filter assembly, and a base cavity for collecting the liquid. The filter assembly consists of nitrate cellulose membrane filter paper with selected pore size, a wire cloth-stainless steel, and a perforated solid steel disc. The filter assembly was placed on the top of the base cavity. The wire cloth-stainless steel was used to keep the filter paper from rupture. Cylinder, filter assembly, and base were tightly sealed by thread and O-ring.

A volume of 175 ml infiltrate was poured into the cylinder to make a consolidated body 6 mm in thickness by pressure infiltration. A MTS testing machine set at constant crosshead speeds (infiltration rates) during infiltrations was used to provide the infiltration pressure on the plunger. The use of a constant crosshead speed insured a gradual increase in pressure, and allowed the alumina fibres and particles to consolidate uniformly, and to prevent the filter paper from rupture. For composites with V_f of 8.1%, crosshead speeds were set at 2, 4 and 7 mm min^{-1} in order to study the effect of infiltration rates on composite green density. Maximum infiltration pressure was reached when the infiltration process stops. Both maximum infiltration pressures and composite green densities were recorded.

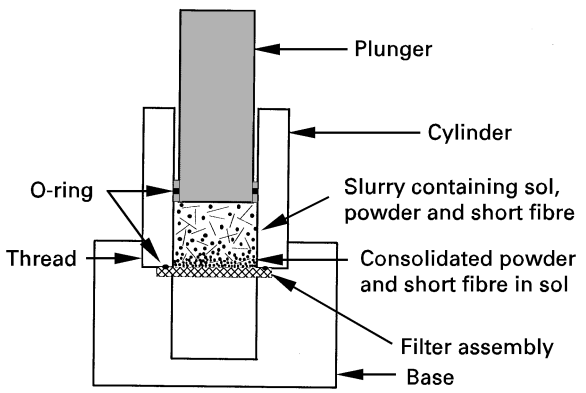

Figure 1 Schematic diagram of pressure infiltration apparatus for consolidation of the short fibre reinforced ceramic matrix composites.

2.3. Drying and hot press

After infiltration, the specimen was ejected and dried in an oven at 58 °C for 24 h. The weight change was measured in an interval of 30 min during drying in order to get the drying rate curve. The composite green density was calculated from its dimensions and weight after drying.

After drying, the green composite was hot pressed in a furnace (FCPHP-R-5, Fret-20, High multi 5000, Multi-purpose High Temperature Furnace, Japan) under temperature 1600 °C and pressure 588 N cm^{-2} by flowing nitrogen gas. After hot pressing, the percentage theoretical density of sintered composites were measured.

2.4. Characterization of composites

In order to facilitate the cutting of green composites for observation, the composites were soaked in cyanoacrylate adhesive to protect their microstructure. Sintered composites were also soaked in epoxy resin and then cured at 60 °C for about 6 h, then cut as specimen. Both green and sintered composites were examined by a scanning electron microscope.

The indentation fracture technique was adopted to determine the fracture toughness of composite materials. The Vickers diamond pyramid indenter was used to produce the crack patterns onto the polished cross-section of specimen. The indentation load was 5 kg, which provides consistent indentation patterns with radial crack lengths substantially larger than the indentation diagonals. Thus, fracture toughness can be calculated by measuring the lengths of diagonals and radial cracks. The following equation [9, 10] was used to evaluate fracture toughness of the short fibre alumina/alumina composites

$$K_{IC} = \ell_v^R (E/H)^{1/2} (P/c^{3/2}) \quad (1)$$

where ℓ_v^R is a constant around 0.016, E is Young's modulus, H is Vicker's hardness, P is indentation load, and c is half of the crack length.

A three-point bending test was adopted to measure flexural strength and modulus of composites. The span L, width w, and height h of the specimen were designed to be 40, 3.5 and 2.6 mm, respectively; detailed dimensions were measured for each specimen for further calculation of the strength and modulus. The relationship of applied load (P) versus displacement (δ) were recorded during the test. The ultimate loads were taken for the calculation of flexural strength and modulus. The flexural strength σ_{max} can

be expressed by

$$\sigma_{max} = 3P_{max}L/(2wh^2) \quad (2)$$

and flexural modulus E_1^f can be evaluated by [11]

$$E_1^f = P_{max}L^3/(4wh^3\delta) \quad (3)$$

where P_{max} is the maximum applied load, L is span between two supported points, w and h are width and height of specimen cross-section, respectively, and δ is crosshead displacement.

3. Results and discussion

3.1. Influence of infiltration rate

For composites with fibre volume fraction of 8.1% and particle size of 3 μm, the effect of infiltration rate on green densities and maximum infiltration pressure is shown in Fig. 2. The infiltration rate of 4 mm min^{-1} results in the highest infiltration pressure and highest green density of the composite. This optimal infiltration rate implies that there is equilibrium between particles packing strength and applied load. But for lower (2 mm min^{-1}) or higher (7 mm min^{-1}) infiltration rates, the green densities and infiltration pressures are lower. The corresponding micrographs of composites are shown in Fig. 3a–c for infiltration rates 2, 4 and 7 mm min^{-1}, respectively. As indicated from Fig. 3b, the composite obtained by infiltration rate 4 mm min^{-1} yields a better fibre/particle packing and therefore a higher density, while composites in Fig. 3a and c show worse packing as well as lower densities.

Kuhn *et al.* [12] have observed the packing of particles in which a balance can be reached between the applied load and the strength of the particle network. If the load increases up to a critical value, the particle would be rearranged. Thus, the particle would be forced to snap and slip into the voids inside the network, resulting in an increase in composite green density, and a new stable particle structure (as shown in Fig. 4). The procedure repeats until further load applies. When the infiltration rate is the lowest

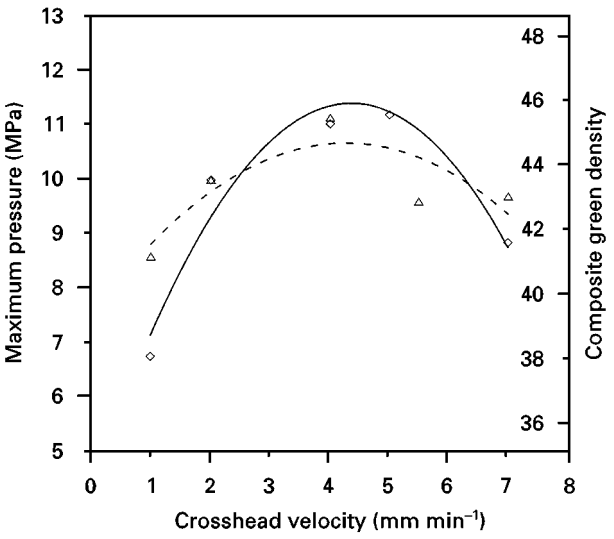

Figure 2 Crosshead velocity versus maximum infiltration pressure (◇) and composite green density (△) for composites with fibre volume fraction of 8.1% and particle size of 3 μm.

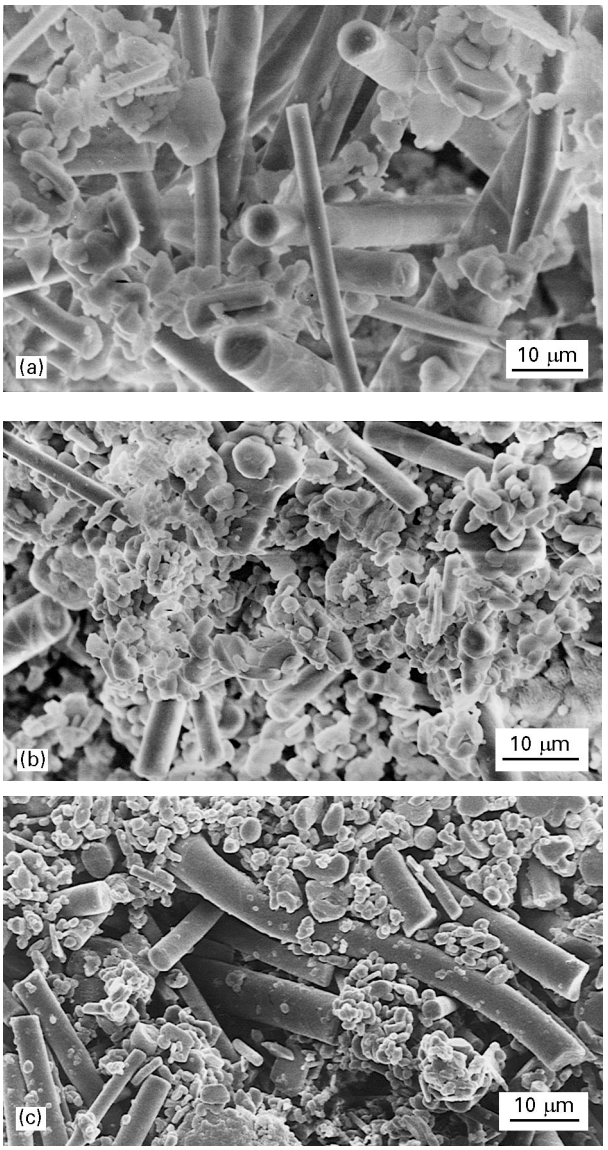

Figure 3 The comparison of green composites with V_f of 8.1% and particle size of 3 μm fabricated by infiltration rates (a) 2 mm min^{-1}; (b) 4 mm min^{-1}; and (c) 7 mm min^{-1}.

(= 2 mm min^{-1}), green density and maximum infiltration pressure decrease. It was because the plunger could not offer enough pressure to overcome constraint of fibres on consolidation, and the pressure is not high enough to rearrange a dense particle packing; thus, the packing of fibres and particles is loose. Furthermore the loosely packed fibres and particles result in higher permeability, lower infiltration pressure, and lower composite green density. When the infiltration rate is the highest (= 7 mm min^{-1}), the packing of particles and fibres is likely to be irregular because the flow speed of solvent is so fast that particles cannot achieve their best packing position. Furthermore, the fast flow of solvent induces large pores around fibres (see Fig. 3c), resulting in a lower composite density and infiltration pressure.

During the infiltration experiment, the swelling of green composites was observed which significantly influences their density. The swelling of green composites was evaluated by comparing the thickness of composites after drying to the designed thickness of

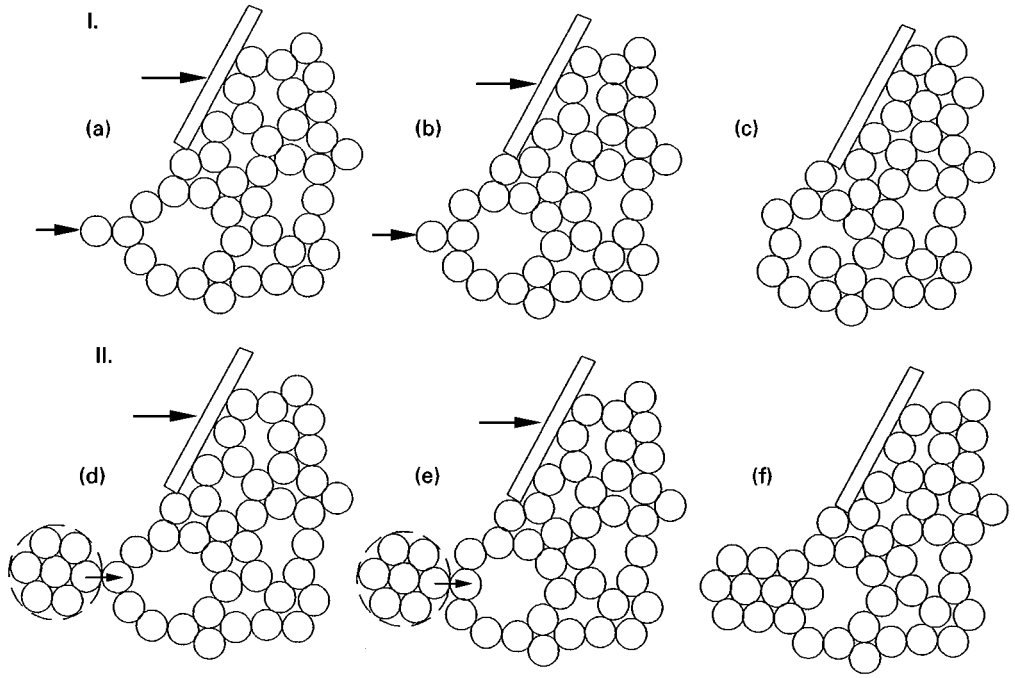

Figure 4 Schematic of packing process with particles and fibres. (I) dispersed state. (a) → (b) → (c), the slurry has strong repulsion interparticle potentials with better packing effect. (II) flocced state. (d) → (e) → (f), the slurry has strong attractive interparticle potentials with bad packing effect.

6 mm. After drying, the thickness of composites with particle size of 3 μm and V_f of 8.1% were found to be 6.6, 6.5 and 6.9 mm for infiltration rates 2, 4 and 7 mm min^{-1}, respectively. The swelling is due to fibre–fibre interactions. The swelling effect offers the additional evidence for the results of densities that are described above.

3.2. Influence of fibre volume fraction and particle size

The influence of fibre volume fraction (V_f) on green density and maximum infiltration pressure of the composite is shown in Table I. Most of the maximum infiltration pressures decrease with increasing V_f. It is because that significant amount of fibres were entangled for the composite with higher V_f, resulting in large voids among particles. Thus, permeability of the composite increases and pressure decreases. Similarly, a higher fibre volume fraction results in a lower composite green density. This is due to fibre–fibre interactions and fibre constraint on particle packing. These effects can lead to the swelling of the green composite and reduce green density. As shown in Fig. 5, the amount of swelling of green composites increases as fibre volume fraction increases. The amount of swelling was evaluated by linear expansion ratio (LER), where LER $= (t_2 - t_1)/t_2$, t_2 is thickness of green composites after drying, and t_1 (6 mm) is designed thickness of green composites. The result in Fig. 5 implies that the increase of V_f leads to more fibre–fibre interactions. Once the green composites are released from the mould, fibres expand without the constraint of infiltration pressure. The amount of expansion is proportional to V_f. This can be demonstrated by the comparison between Fig. 6 and Fig. 3b, with V_f of 25.4 and 8.1%, respectively. In Fig. 6, more fibre–fibre interactions result in large pores among fibres and loosely packed particles; but fibres and particles in the composite with lower V_f can pack more densely, as shown in Fig. 3b.

The effect of particle size on the processing of composite is shown in Table I. The results show that composite green density is proportional and maximum infiltration pressure is inversely proportional to the particle size as well as diameter ratio R of particle to fibre. During the processing, the sedimentation of both short fibres and particles were observed. It is

TABLE I The influence of fibre volume fraction and particle size on maximum infiltration pressure and green density of composites

Composite type	Density %			Maximum pressure (MPa)		
	Particle size			Particle size		
	3 μm ($R = 1$)	1 μm ($R = 1/3$)	0.45 μm ($R = 0.15$)	3 μm ($R = 1$)	1 μm ($R = 1/3$)	0.45 μm ($R = 0.15$)
$V_f = 8.1$ vol%	55.9	52.4	43.3	11.0	14.3	22.6
$V_f = 16.6$ vol%	53.8	49.8	35.6	12.2	13.2	21.7
$V_f = 25.4$ vol%	48.2	48.6	30.2	6.9	11.6	15.7

R: diameter ratio of particle to fibre.

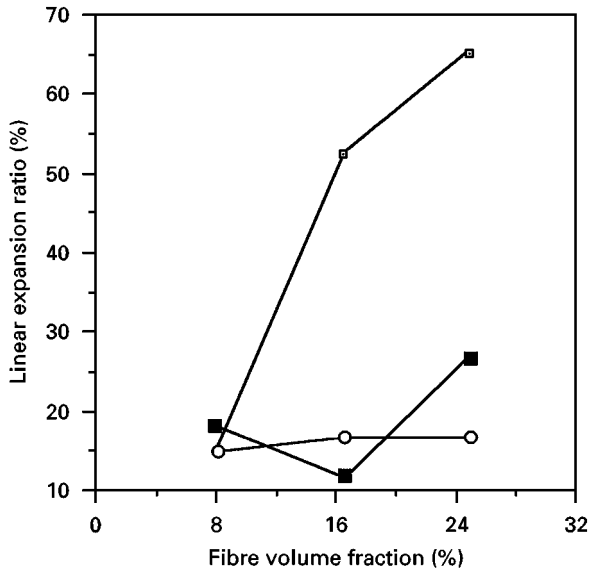

Figure 5 The influence of fibre volume fraction and particle size on linear expansion ratio of green composites. (□) 0.45 μm; (○) 1.0 μm; (■) 3.0 μm.

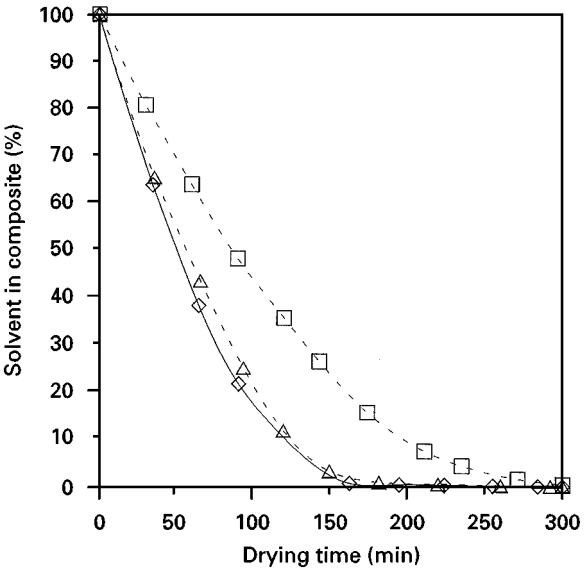

Figure 7 The relationship for drying time versus solvent content of composites with V_f of 8.1% and different particle sizes fabricated by infiltration rate 4 mm min^{-1}. (◇) 3 μm; (△) 1.0 μm; (□) 0.45 μm.

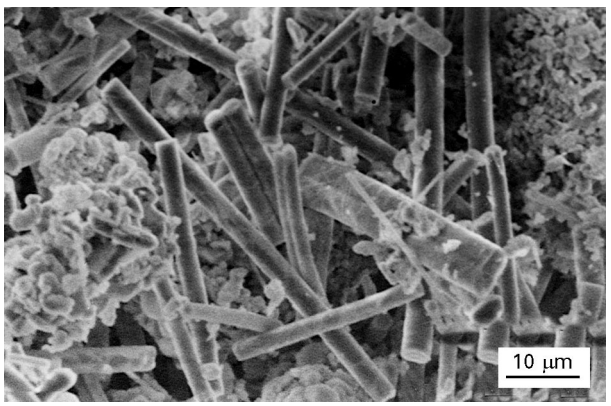

Figure 6 The green composite with V_f of 25.4% and particle size of 3 μm fabricated by infiltration rate 4 mm min^{-1}.

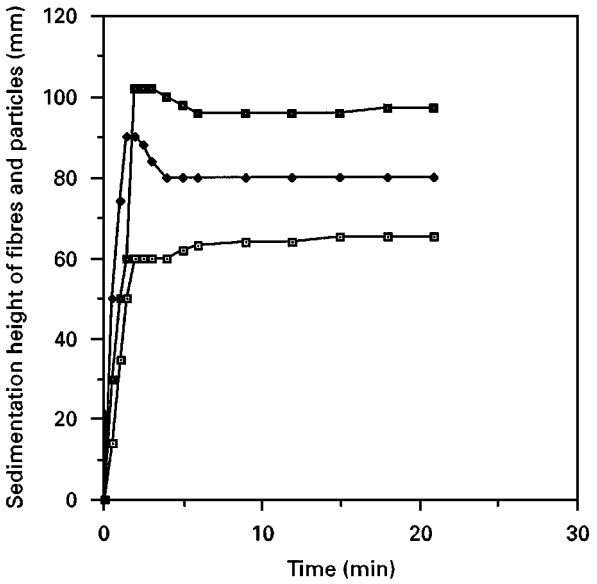

Figure 8 The effect of sol viscosity on sedimentation of infiltrate with V_f of 8.1% and particle size of 3 μm. (□) 0.0405 Pa s; (◆) 0.0507 Pa s; (■) 0.0861 Pa s.

inferred that the sedimentation rate of both short fibres and larger particles is similar such that they still can pack together to obtain a green composite without large swelling. But the higher sedimentation rate of short fibres than smaller particles results in serious fibre–fibre interaction in the fibre packing layer, although particles can pack above the fibre layer. The consequence is significant swelling of fibre layer as well as lower green density. This result can be found from Fig. 5 indicating that the smaller particles lead to larger swelling of green composites. Fig. 7 shows that the drying rate decreases with the decrease of particle sizes for the composite with V_f of 8.1%, showing that permeability is proportional to square of particle diameter [13].

3.3. Influence of sol viscosity

As shown in Table II, a higher sol viscosity leads to lower composite green density and infiltration pressure. The sol viscosity influences sedimentation of infiltrate which further affects particle packing. Therefore an experiment of effect of sol viscosity on sedimentation of infiltrate was conducted. The results are shown in Fig. 8. The sedimentation height of fibres and particles increases with the increase of sol viscosity. During the infiltration process, very fine silica particles in the sol with higher viscosity serves as a strong binder to connect alumina particles or alumina fibres as agglomerates, therefore, they easily result in sedimentation. The above effect leads to the results shown in Table II in which both green densities and maximum infiltration pressures decrease as sol viscosities increase. When the sedimentation height of fibres and particles is large, density of randomly packed particles in the sedimentation layer is low because of a segregation effect. Therefore, the thicker the sedimentation layer, the lower is the green density of the composite. In addition, the permeability of thick

TABLE II The influence of sol viscosity on composite green density and maximum infiltration pressure for the composite with V_f of 8.1%

Viscosity of sol (Pa s)	Composite green density (%)	Maximum pressure (MPa)	Crosshead speed (mm min^{-1})
0.041 ± 0.001	45.4	11.0	4
0.051 ± 0.001	43.8	8.4	4
0.086 ± 0.001	43.7	6.9	4

sedimentation layer is high such that the corresponding maximum infiltration pressure is low. This result is consistent with Darcy's law [14], since Darcy's law implies that a compact's resistance to fluid flow is caused by the viscous flow of fluid over the particles of the compact. Because under constant infiltration rate, the increase of sol viscosity and the decrease of maximum infiltration pressure imply that the permeability increases, which is compatible with the results described above.

3.4. Mechanical properties

Table III depicts the results of fracture toughness of short fibre alumina/alumina composites. In general, fracture toughness is achieved by modifying the microstructure of the matrix to reduce stresses near the crack tip. For composites with particle size of 1 μm and V_f of 8.1 and 16.6%, fracture toughness is proportional to V_f, indicating that short fibres offer major fracture resistance by the following mechanisms: microcracking, load transfer, bridging, and crack deflection. The fracture toughness of composites is at most 38% higher than that of monolithic alumina. However, with V_f of 25.4%, fracture toughness of composites decrease, because of significant fibre entanglement. The limited improvement of fracture toughness may be explained as follows. Silica sol in the infiltrate may react with both alumina fibres and particles and produce mullite with lower melting point, which is beneficial for interfacial strength but worse for fracture toughness of the composite. This can be demonstrated by the observation that fibre pull-outs were seldom found in the fracture surface of the specimen. Another possible fracture resistance mechanism which is not offered by short fibres is energy absorbing pores. The presence of porosity in the samples could

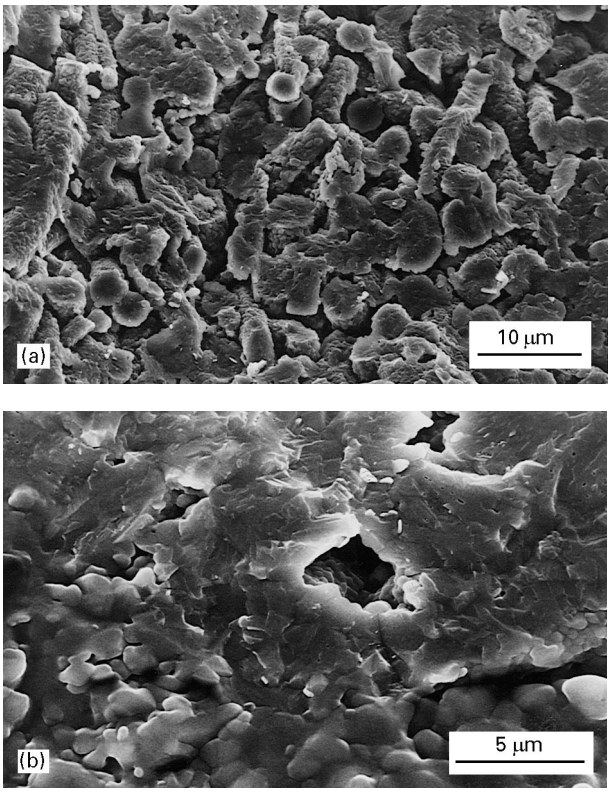

Figure 9 Sintered composites showing different pore size, shape, and distribution with particle sizes (a) 0.5 μm and (b) 1 μm.

make brittle fracture more tortuous, and therefore raise the toughness somewhat, because the energy of sharp cracks would be dissipated when they meet the pores. Some of the pores were observed for composites with particle size of 0.5 μm (Fig. 9a), and with particle size of 1.0 μm (Fig. 9b). However, the quantitative effect of pore size, shape, and distribution on fracture toughness of composites need to be further studied. Particle size also influences fracture toughness of composites as shown in Table III. The composite composed of smaller particles has higher density and higher fracture toughness as fewer number of residual pores in the composite reduces the probability of crack initiation during the indentation test.

The results for flexural strength and modulus are shown in Table IV. Both flexural strength and modulus increase as fibre volume fraction increases, indicating that more fibres strengthen the composites better by crack bridging and deflection. Fibre pull-outs was seldom found in the fracture surface of the

TABLE III The results of fracture toughness using indentation fracture technique

$Al_2O_{3(f)}/Al_2O_{3(m)}$ Vol %	Powder size (μm)	K_{IC} (MPa m$^{1/2}$)			H_V (GPa)	Green density (%TD)	Final density (%TD)
		Matrix	Composite	Increase (%)			
8.1	0.45	4.0	5.5 ± 0.5	38	16.0	51.8	92.1
8.1	1	4.0	4.6 ± 0.3	16	13.1	55.0	82.4
16.6	1	4.0	5.3 ± 0.6	33	13.7	52.2	94.0
25.4	1	4.0	3.8 ± 0.4	−5	17.0	51.8	97.6

TD: theoretical ensity.

TABLE IV The results of mechanical properties

Composite type	Flexural strength (MPa)	Flexural modulus (GPa)
8.1 vol % fibres	293.2 ± 51.2	264.9 ± 35.5
25.4 vol % fibres	388.8 ± 29.3	293.7 ± 29.9

Fibre, modulus of elasticity = 300 GPa; Poisson's ratio = 0.136.
Matrix; modulus of elasticity = 343 GPa; Poisson's ratio = 0.22.

specimen; this means that the specimen have good interfacial strength because of mullite phase. The result is consistent with the data shown in Table IV that composite strength is proportional to fibre volume fraction.

4. Conclusions

Pressure infiltration is a viable method to fabricate dense short fibre alumina/alumina composites with well-controlled properties by mixing silica sol, alumina particles, and short alumina fibres. For the composite with fibre/particle diameter ratio R of 1 and V_f of 8.1%, the optimal infiltration rate for highest green density is 4 mm min^{-1}. Both higher or lower infiltration rates result in lower densities. A higher fibre volume fraction leads to a lower composite green density. Smaller particles result in lower composite green density and lower drying rate. When infiltrate viscosity increases, green density and maximum infiltrate pressure of composites decrease due to sedimentation. Fracture toughness of composites with V_f of 8.1 and 16.6% are approximately 16 and 38% higher than those of monolithic ceramics, respectively. Smaller particles lead to less residual pores and result in higher fracture toughness due to lower possibility of crack initiation. Flexural strengths of composites with V_f of 8.1 and 25.4% are 293.2 and 388.8 MPa respectively.

Acknowledgements

The authors are grateful to National Science Council, Taiwan for financial support under contracts NSC 83-0405-E-035-017 and NSC 84-2216-E-035-027.

References

1. S. CHIOU and H. T. HAHN, *J. Amer. Ceram. Soc.* **77** (1994) 155.
2. B. I. LEE and L. L. HENCH, in "Science of ceramic chemical processing", edited by L. L. Hench and D. R. Ulrich (John Wiley & Sons, New York, 1986) p. 231.
3. D. E. CLARK, in "Science of ceramic chemical processing", edited by L. L. Hench and D. R. Ulrich (John Wiley & Sons, New York, 1986) p. 237.
4. H. K. LIU and A. PARVIZI-MAJIDI, *Ceram. Engng Sci. Proc.* **13** (1992) 642.
5. B. V. VELAMAKANNI and F. F. LANGE, *J. Amer. Ceram. Soc.* **74** (1991) 166.
6. F. F. LANGE, D. C. C. LAM and O. SUDRE, "Materials Research Society Proceedings" Vol. 155 (Materials Research Society, Pittsburgh, 1989) p. 309.
7. J.C. CHANG, F. F. LANGE, D. S. PEARSON and J. P. POLLINGER, *J. Amer. Ceram. Soc.* **77** (1994) 1357.
8. L. C. KLEIN, *Ann. Rev. Mater. Sci.* **15** (1985) 227.
9. G. R. ANSTIS, P. CHANTIKUL, B. R. LAWN and D. B. MARSHALL. *J. Amer. Ceram. Soc.* **64** (1981) 533.
10. K. XIA and T. G. LANGDON, *J. Mater. Sci.* **29** (1994) 5219.
11. L. A. CARISSON and R. B. PIPES, "Experimental characterization of advanced composite materials", (Prentice-Hall, New Jersey, 1987) Chapter 7.
12. L. T. KUHN, R. M. MCMEEKING and F. F. LANGE, *J. Amer. Ceram. Soc.* **74** (1991) 682.
13. H. K. LIU, *J. Mater. Sci.* **31** (1996) 5093.
14. F. A. L. DULLIEN, "Porous media: fluid transport and pore structure" (Academic Press, New York, 1979) Chapter 4.

Received 17 December 1996
and accepted 17 December 1997